*sustainability*

MDPI

*Article*

# A Multi-Objective Optimization Method of Sustainable Wind–Photovoltaic–Hydro Systems Considering Source–Grid Coordination

**Qin Shen [1,2,3], Li Mo [1,2,3,*], Zixuan Liu [1,2,3], Xutong Sun [1,2,3], Guanjun Liu [1,2,3] and Yongchuan Zhang [1,2,3]**

1 School of Civil and Hydraulic Engineering, Huazhong University of Science and Technology, Wuhan 430074, China; shenqin@hust.edu.cn (Q.S.); zixuan_liu@hust.edu.cn (Z.L.); m202371715@hust.edu.cn (X.S.); liugj@hust.edu.cn (G.L.); yczhang@hust.edu.cn (Y.Z.)
2 Hubei Key Laboratory of Digital River Basin Science and Technology, Huazhong University of Science and Technology, Wuhan 430074, China
3 Institute of Water Resources and Hydropower, Huazhong University of Science and Technology, Wuhan 430074, China
* Correspondence: moli@hust.edu.cn

**Abstract:** Hydropower compensating for wind and solar power is an efficient approach to overcoming challenges in the integration of sustainable energy. Our study proposes a multi-objective scheduling model for the complementary operation of wind–photovoltaic–hydro systems. The model aims to maximize the total generation while minimizing the mean square deviation of the system output and grid load. Taking wind and solar bases and key peak-shaving cascade hydropower stations in Hubei Province as a case study, various multi-objective Pareto solution sets were obtained for different scheduling periods. The analysis dissects the relationship between total generation and the stability of residual load after adjustment by the wind–photovoltaic–hydro systems. Furthermore, the study analyzes the role that a complementary system should play in the power grid and discusses the effect of cascade hydropower scheduling methods on the operational characteristics of multi-energy complementary systems.

**Keywords:** wind–photovoltaic–hydro system; power generation; load fluctuation; complementary mechanism; Pareto set

check for updates

**Citation:** Shen, Q.; Mo, L.; Liu, Z.; Sun, X.; Liu, G.; Zhang, Y. A Multi-Objective Optimization Method of Sustainable Wind–Photovoltaic–Hydro Systems Considering Source–Grid Coordination. *Sustainability* **2024**, *16*, 61. https://doi.org/10.3390/su16010061

Academic Editor: Jiageng Ruan

Received: 2 December 2023
Revised: 15 December 2023
Accepted: 18 December 2023
Published: 20 December 2023

**Copyright:** © 2023 by the authors. Licensee MDPI, Basel, Switzerland. This article is an open access article distributed under the terms and conditions of the Creative Commons Attribution (CC BY) license (https://creativecommons.org/licenses/by/4.0/).

## 1. Introduction

With the depletion of traditional fossil fuels, climate change, and the global transition towards cleaner energy sources, renewable energies such as wind, solar, and hydropower have gained significant attention worldwide [1]. In response, many countries, exemplified by China, have vigorously developed wind and photovoltaic (PV) renewable energy resources. To implement the action plan for carbon dioxide peaking before 2030 [2], China plans to initiate pilot programs for carbon peaking in 100 cities and zones across the country, addressing obstacles that hinder the nation's progress in green and low-carbon development. The objective is to investigate strategies for achieving carbon peaking tailored to diverse regions [3]. However, the stochastic, volatile, intermittent, and uncertain characteristics of wind and photovoltaic power generation present substantial challenges to the stability of the power grid [4]. With the growing integration of renewable energy and its increasing penetration rate, the impact on the power grid is expected to intensify without proper regulation, particularly given the ongoing development of energy storage technologies [5]. Hydropower, characterized by advantages like rapid start-up and excellent regulation performance, has been recognized as an ideal energy source for mitigating the fluctuations in wind and photovoltaic power outputs [6]. Therefore, the complementary integration of wind–photovoltaic–hydropower systems (WPHSs) is acknowledged

as an efficient strategy to address the challenges of grid integration for wind and solar consumption [7].

Optimization scheduling of multi-energy complementary systems is a dispatching mode that packages the output of each subsystem to the grid according to resource conditions and typical characteristics to meet terminal electricity demand [8]. In recent years, research on typical multi-energy complementarity has focused on wind–photovoltaic complementarity, hydro–wind complementarity, hydro–photovoltaic complementarity, and wind–solar–hydro complementarity, among others [9]. Common scheduling objectives can be divided into station-side goals and grid-side goals. Station-side goals include maximizing power generation [10], water resource supply [11], and minimizing output fluctuations [12]. Grid-side goals typically include minimizing residual load variance [13], minimizing maximum residual load [14], and economic benefits. Due to the low cost of WPHSs, particularly in the short term, ensuring overall economic efficiency is crucial to enhancing the enthusiasm for cascade hydropower participation in complementary systems [15,16]. Therefore, the primary objective for most complementary systems is to maximize power generation. The joint operation with wind and solar energy also brings new challenges to reservoir scheduling, and cascade hydropower needs to coordinate with the peak load operation of the new power system with wind and photovoltaic integration.

Previous research has primarily focused on single-objective models. For example, Jin et al. [17] proposed a combined scheduling framework for wind, solar, and hydropower, with the objective of minimizing the residual mean anomaly. The model was subsequently transformed into a mixed-integer linear programming problem for resolution. This demonstrated that the optimal development of wind and solar power could effectively harness their complementarity, thereby mitigating the variability in hydropower output across various time scales. Considering wind and solar uncertainty, Wang et al. [18] made a short-term peak shaving model for a water-pumped hydro storage system, incorporating considerations of uncertainty and applying a parallel particle swarm optimization algorithm to solve the proposed model, and verified its efficacy using the water–wind–solar hybrid system within the East China Power Grid. Based on stochastic programming theory, Zhang et al. [19] developed a peak shaving model utilizing the expected value of the variance of the system's remaining load. The model was solved using the commercial solver LINGO18.0. However, while single-objective scheduling models have made significant progress in optimizing water resources, their limitations have gradually become apparent as new challenges in water area management, such as water level control, grid coordination, and ecological protection. Multi-objective scheduling models have various advantages over single-objective models, covering a more comprehensive and flexible consideration of different aspects of water area resource management requirements. Wang et al. [18] formulated a multi-objective scheduling model to enhance the complementarity of hydro–wind–solar systems, aiming to maximize power generation while minimizing output fluctuations. The validity of the model was confirmed through a case study involving the power grid of a southwestern prefecture-level city. This validation showcased the effectiveness of the model, and the study delved into the complementary mechanisms of WPHSs. Taking into account the complementarity between wind and solar energy, a comprehensive system capacity allocation model was established to minimize cumulative fluctuations [20]. The study analyzed the complementarity characteristics between different energy sources using a case study in Qinghai Province. Li et al. [21] employed an autoregressive integrated moving average (ARIMA) model to generate typical days, considering weather factors. The study devised a model with the objective of minimizing supply risk and maximizing economic benefits. Results under different scenarios demonstrated that multi-energy complementary systems do not affect stability but increase overall economic benefits. To investigate the adjusting capacity of various scales of hydropower in relation to wind and photovoltaic power, a two-layer model was suggested [22]. This model aimed to coordinate cascade hydropower with adjacent wind and photovoltaic facilities. The research revealed that 90% of fluctuations in wind and solar power output could be

mitigated through local hydropower supplementation. This implies that the coordinated operation of cascade hydropower with wind and photovoltaic power holds promise as an effective approach to emissions reduction in power systems. In [23], the advantages and drawbacks of the collaborative operation of the hybrid wind–photovoltaic–hydropower system are assessed. In [24], a short-term multi-objective dispatching model for coordinating wind–photovoltaic–hydro hybrid power generation is presented. Objectives include maximizing new energy utilization, closely aligning with the grid's load curve, and minimizing cascade discarded water. In [25], the study focused on the Yalong River Wind-PV-Hydro clean energy base to investigate the output complementarity principles and characteristics of wind farms, photovoltaic power plants, and hydropower stations. Subsequently, an optimization scheduling model was developed with the goal of minimizing the waste of wind and photovoltaic power while maximizing energy storage in cascade hydropower stations. Hence, it is worthwhile to delve deeper into the short-term optimization of basin cascade hydro–wind–photovoltaic complementary systems, warranting further exploration and investigation.

Combined with the research progress at home and abroad, the current research pays little attention to the complementary role assignment of cascade hydropower stations in hydro–new energy complementary systems, and there is a lack of research on the role of hydro–new energy complementary systems in the power grid and the influence of the relative position of cascade hydropower stations on the hydro–new energy complementary operation characteristics. While recent research has made progress, there are still some shortcomings that need to be overcome. These include the coordination issues faced by wind and solar new energy after grid connection, specifically the coordination between power plant efficiency and grid demand. It requires providing decision-makers with more comprehensive optimization decision support. Against the background of multi-energy complementarity, further exploration is needed into the correlation between overall power generation and the stability of residual load. Additionally, the role of cascade hydropower in multi-energy coordination mechanisms needs to be investigated. Therefore, to address the aforementioned issues, this study presents a multi-objective short-term optimization model for WPHSs, aiming to maximize total generation benefits while minimizing the disparity between the output of the complementary system and load processes. By applying the model to typical days in different scheduling periods, the Pareto solution set considering the preferences of different decision-makers is obtained. Multi-objective scheduling offers the advantage of simultaneously optimizing various conflicting objectives, allowing for a balanced and comprehensive approach to decision making. The correlation among total power generation, output, and load processes is analyzed. This paper explores the effect of cascade hydropower scheduling on the operational characteristics of multi-energy complementary systems.

The rest of this study is structured as follows. In Section 2, the proposed short-term multi-objective scheduling model is described in detail, which incorporates the calculation of power generation from WPHSs, objective functions, and constraints. Section 3 presents the model solution algorithm. Section 4 shows the study area, experimental findings, and a detailed discussion. Section 5 provides conclusions and corresponding suggestions for future applications.

## 2. Multi-Objective Optimization Model Formulation

In this section, a comprehensive introduction to power output calculation methods, the objective functions, and constraints within the multi-objective optimization model for WPHSs is presented.

### 2.1. Power Output Calculation Methods

(1) Wind power generation

Wind power is primarily associated with wind speed [26], air density, swept area, and fan efficiency. The equation is expressed as follows:

$$N = \frac{1}{2}\rho A C_p v^3 \tag{1}$$

where $N$ represents the output of wind plants, $\rho$ represents the air density, $A$ denotes the area swept by the turbine blades, $C_p$ represents the power coefficient, and $v$ represents the wind speed.

(2) Photovoltaic power generation

Photovoltaic power generation primarily leverages the photovoltaic effect of semiconductor materials, converting solar energy directly into clean electrical energy. The calculation of photovoltaic power output can be expressed as: [27]

$$P = \eta A G[1 - \partial_T(T - T_{\text{ref}})] \tag{2}$$

where $P$ represents the photovoltaic power generation (W); $\eta$, $A$, and $\partial_T$ denote the conversion efficiency, area ($m^2$), and temperature coefficient of the photovoltaic panel, respectively; $G$ represents solar radiation ($W/m^2$); $T$ is the temperature of the photovoltaic panel cells, and $T_{\text{ref}}$ is the standard cell temperature.

(3) Hydropower generation

Hydropower generation is primarily influenced by the difference in water levels between upstream and downstream [28]. The equation is expressed as follows:

$$N = KhQH \tag{3}$$

where $N$ denotes the hydropower output, $Q$ represents the outflow, $H$ represents the net water head of the hydropower plant, and $K_h$ represents the output coefficient.

### 2.2. Objective Functions

The multi-energy complementary system needs to consider many factors such as power generation efficiency and power load demand. Therefore, this study aims to propose an optimal dispatch model for the WPHS with the objective of maximizing the total power generation of the complementary system and minimizing the mean square error of residual load.

(1) Hydropower station side: Maximizing the total power generation

The economic benefits of WPHSs are intricately linked to the system's output, so the first object is to maximize the total system output. The formula is as follows:

$$\max F_1 = \max\{\sum_{t=1}^{T} N_t \cdot \Delta t\} \tag{4}$$

$$N_t = \sum_{i=1}^{M_w} N_{w,i,t} + \sum_{j=1}^{M_s} N_{s,j,t} + \sum_{k=1}^{M_h} N_{h,k,t} \tag{5}$$

where $F_1$ represents the overall power generation of the complementary model; $N = [N_1, N_2, \cdots, N_T]$ represents the output process of the WHPSs; $N_t$ is the overall output of the $t$-th period; $N_{w,i,t}$ is the output of the $i$-th wind power plant during the $t$-th period; $N_{s,j,t}$ is the output of the $j$-th photovoltaic power plant during the $t$-th period; $N_{h,k,t}$ is the output of the $k$-th hydropower plant during the $t$-th period; $M_w$, $M_s$, and $M_h$ represent the number of wind plants, photovoltaic plants, and hydropower plants in the complementary

system, respectively; $T$ and $\Delta t$ are respectively the overall number of periods and the single period in the dispatch period.

(2) Power grid side: Minimizing the mean square error of the residual load

$$\begin{aligned} &\min F_2 = \min\left\{\sqrt{\frac{1}{T}\sum_{t=1}^{T}(R_t-\overline{R})^2}\right\} \\ &\begin{cases} R_t = P_t - N_t \\ \overline{R} = \frac{1}{T}\sum_{t=1}^{T} R_t \end{cases} \end{aligned} \tag{6}$$

where $F_2$ denotes the mean square error of the grid residual load after peak shaving by the WPHS; $P_t$ denotes the grid load; $R_t$ denotes the residual load after deducting the output of wind power, photovoltaic power, and hydropower during period $t$; $\overline{R}$ denotes the average value of residual load.

### *2.3. Constraints*

(1) Water volume balance constraints

$$V_{k,t+1} = V_{k,t} + (I_{k,t} - Q_{k,t} - Ev_{k,t}) \cdot \Delta t \tag{7}$$

where $V_{k,t}$ and $V_{k,t+1}$ denote, respectively, the beginning and ending storage volumes of the $k$-th reservoir during the $t$-th period; $I_{k,t}$, $Q_{k,t}$, and $Ev_{k,t}$ represent the inflow, outflow, and evaporation loss of the $k$-th reservoir in the $t$-th period, respectively; $\Delta t$ represents the time interval in each period.

(2) Water level constraints

$$Z_{u,k,t}^{\min} \le Z_{u,k,t} \le Z_{u,k,t}^{\max}, \tag{8}$$

where $Z_{u,k,t}$ represents the water level upstream of the $k$-th reservoir during the $t$-th period; $Z_{u,k,t}^{\max}$ and $Z_{u,k,t}^{\min}$ respectively represent the upper and lower bounds of the water level upstream of the corresponding reservoir during the corresponding period.

(3) Reservoir discharge flow constraints

$$Q_{k,t}^{\min} \le Q_{k,t} \le Q_{k,t}^{\max} \tag{9}$$

where $Q_{k,t}$ represents the total discharge of the $k$-th reservoir during the $t$-th period, comprising both power generation flow and abandoned water flow; $Q_{k,t}^{\max}$ and $Q_{k,t}^{\min}$ represent the upper and lower limits of the total discharge of the corresponding reservoir in the corresponding period, respectively.

(4) Hydropower plant output constraints

$$N_{h,k,t}^{\min} \le N_{h,k,t} \le N_{h,k,t}^{\max} \tag{10}$$

where $N_{h,k,t}$ denotes the power output of the $k$-th reservoir during the $t$-th period; $N_{h,k,t}^{\max}$ and $N_{h,k,t}^{\min}$ denote the upper and lower bounds, respectively, of the corresponding reservoir's power generation output in the corresponding period.

(5) Wind speed constraints

$$v_{i,t}^{\min} \le v_{i,t} \le v_{i,t}^{\max} \tag{11}$$

where $v_{i,t}$ is the wind speed of the $i$-th wind farm in the $t$-th period; $v_{i,t}^{\min}$ and $v_{i,t}^{\max}$ are respectively the incoming and outgoing wind speeds of the corresponding wind power station in the corresponding period.

(6) Photovoltaic capacity constraints

$$N_{s,j,t}^{\min} \leq N_{s,j,t} \leq N_{s,j,t}^{\max} \tag{12}$$

where $N_{s,j,t}$ denotes the power output of the $j$-th photovoltaic plant during the $t$-th period; $N_{s,j,t}^{\max}$ and $N_{s,j,t}^{\min}$ denote the upper and lower bounds, respectively, of the generating plate capacity of the corresponding photoelectric field in the corresponding period.

## 3. Optimization Problem Solution Using a Multi-Objective Cultured Evolutionary Algorithm Based on Decomposition

Given that the objective functions and constraints within the proposed optimization model encompass nonlinear relationships, this model is classified as nonlinear. Common techniques employed in the literature for multi-objective optimization models comprise the linear weighting method, primary objective method, approximation objective method, and various multi-objective optimization algorithms. Compared to the first two traditional methods, multi-objective optimization algorithms excel in handling complex relationships among multiple objectives, providing a more comprehensive and diverse set of Pareto optimal solutions. Through nondominated sorting and evolutionary strategies, multi-objective optimization algorithms are better suited for addressing high-dimensional, nonlinear, multi-modal, and complex constraint-laden problems. They possess the capability of global search, offering decision-makers a richer choice space and balanced solution sets. Therefore, we have adopted the multi-objective cultured evolutionary algorithm based on decomposition to solve the proposed model. The subsequent sections elaborate on the detailed procedures of MOCEA/D.

### *3.1. Multi-Objective Evolutionary Algorithm Based on Decomposition*

The multi-objective evolutionary algorithm based on decomposition (MOEA/D) was first proposed by Zhang and Li [29], which constitutes an evolutionary algorithm employed for the resolution of multi-objective optimization challenges. Its fundamental concept involves decomposing a multi-objective optimization problem into a sequence of single-objective optimization problems and effectively decoupling multiple subproblems through decomposition technology. In MOEA/D, the initial step involves determining sets of weight vectors used to decompose a multi-objective optimization problem into a sequence of single-objective optimization problems.

### *3.2. Cultural Algorithm*

The cultural algorithm (CA) is a two-layer evolutionary mechanism proposed by Robert G. Reynolds in 1994 [30]. Culture serves as a knowledge base that preserves people's past experiences so that future generations can learn experiential knowledge without direct experience in the knowledge base. Unlike the genetic algorithm, which only has a population evolution space, the CA includes two evolution spaces: belief space and population space. The population space and belief space are two distinct evolutionary processes, each maintaining its own sets and evolving autonomously. The population space consistently offers elite individuals to the belief space, while the belief space continually evolves its elite group, thereby influencing the population space group.

### *3.3. Multi-Objective Cultured Evolutionary Algorithm Based on Decomposition*

The multi-objective cultured evolutionary algorithm based on decomposition (MOCEA/D) integrates the MOEA/D algorithm with the CA algorithm, addressing the challenge of the CA algorithm's high complexity in solving high-dimensional target problems. Furthermore, it enhances the MOEA/D algorithm to achieve faster convergence to the optimal solution. The fundamental concept behind the MOCEA/D algorithm is to employ weight vectors for decomposing multi-objective problems and utilize the mutual influence of fields to address problem solving. The flowchart of MOCEA/D is presented in Figure 1. The procedure of the MOCEA/D is outlined as follows:

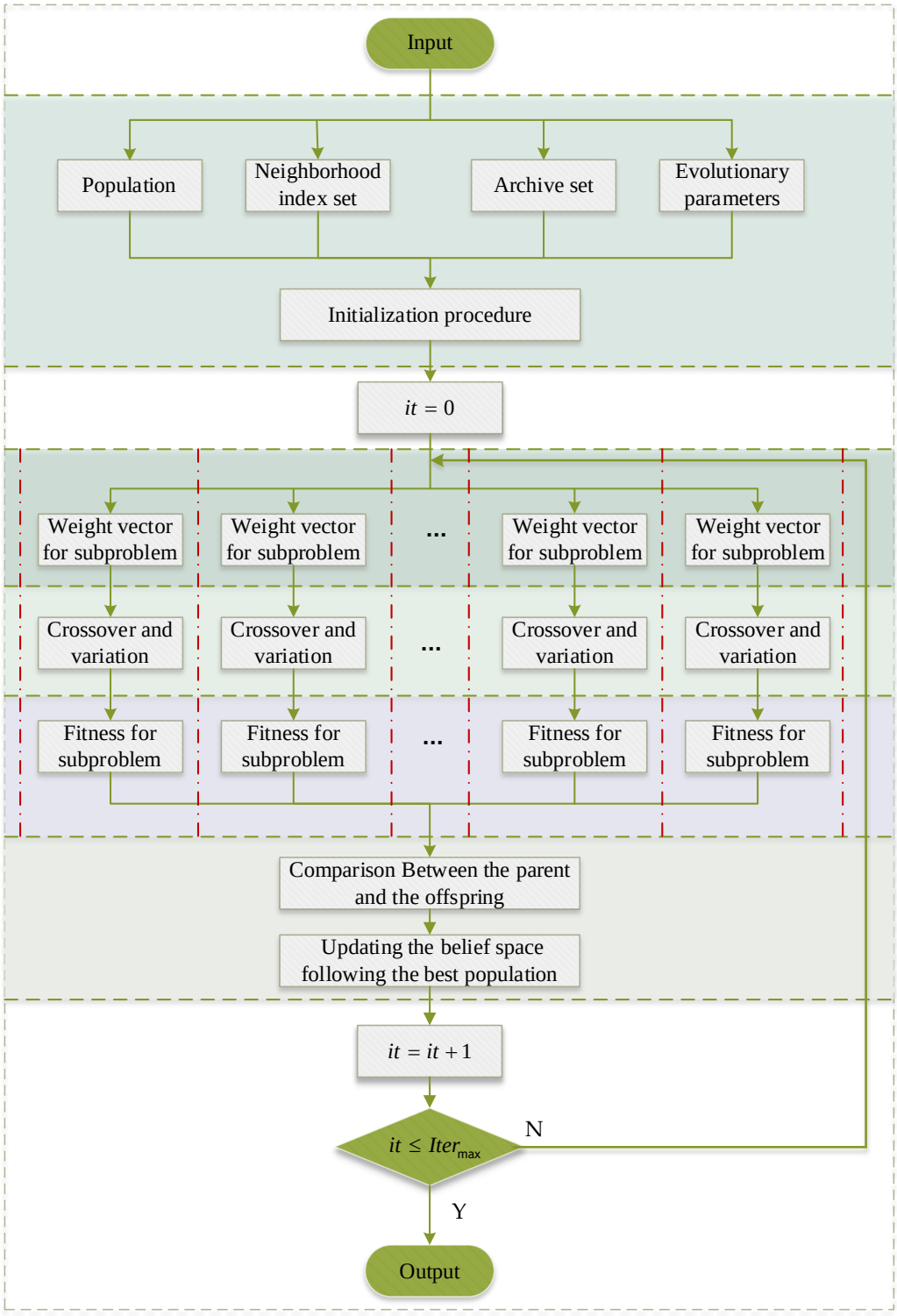



**Figure 1.** The flowchart of MOCEA/D algorithm.

Step 1: Generate weight vectors by alternative methods, and initialize neighborhood index set.

Step 2: Generate the population through the initialization function. The initialization belief space includes the archive set (optimal solution set) and MOCEA/D evolution parameters. MOCEA/D uses differential evolution as an evolutionary algorithm and initializes it within a reasonable range to generate $N$ sets of parameters $F$ and $CR$. Each set of parameters corresponds to the corresponding subproblem $i$.

Step 3: Update the evolution parameters $F$ and $CR$ according to the belief space. For each subproblem $i$, the specific formula is as follows:

$$F = \begin{cases} F_{\min} + rand_1() \bullet (F_{\max} - F_{\min}) rand_2() < \tau_1 \\ F_i \qquad\qquad otherwise \end{cases} \tag{13}$$

$$CR = \begin{cases} CR_{\min} + rand_3() \bullet (CR_{\max} - CR_{\min}) rand_4() < \tau_2 \\ CR_i \qquad\qquad otherwise \end{cases} \tag{14}$$

Step 4: Generate offspring individuals. For each subproblem, I, select parent individuals from the neighborhood population or archive set to perform the regeneration process to generate new offspring (the evolution parameters used in the regeneration process are $F$ and $CR$ obtained in step 3).

Step 5: Update population. For each subproblem $i$, compare the children obtained in step 4 with the parent generation, and update the parent generation scheduling plan. The parent update process is based on the dominance relationship and the penalty function-based boundary intersection (PBI) method.

Step 6: Update belief space. Update evolution parameters and archive sets separately.

Step 7: Iterate through steps 3–6 until the designated number of iterations is achieved.

## 4. Case Study

### *4.1. Research Area*

Hubei Province is located in south-central China and is rich in hydropower, wind power, and photovoltaic resources. It is one of China's important renewable energy power generation bases. With the reform of the power industry and the clean and low-carbon transformation of the energy structure, the installed capacity of new energy in Hubei Province has increased significantly in recent years. Wind stations are mainly concentrated in Enshi, Jingmen, Suizhou, and other places, and photovoltaic power plants are mainly concentrated in Huanggang, Suizhou, Xiangyang, and other cities. Meanwhile, Qingjiang cascade hydropower stations are the main peak-shaving supply of the Hubei Province Power Grid. The Qingjiang River is a primary tributary of the Yangtze River in China, situated in the southwest of Hubei Province. Originating from Lichuan City, it flows into the Yangtze River in Yidu City, covering a total length of 423 km. The Qingjiang River controls a watershed area of 16,700 $km^2$, mostly in mountainous areas with abundant water, with an average flow of 440 $m^3/s$ and a multi-year average runoff of 14.7 billion $m^3/s$. The Qingjiang mainstream cascade hydropower station is developed in three levels. From top to bottom, they are Shuibuya Hydropower Station, Geheyan Hydropower Station, and Gaobazhou Hydropower Station. The fundamental parameters of the Qingjiang cascade hydropower stations are presented in Table 1. A general diagram of WPHSs in Hubei Province is plotted in Figure 2.

**Table 1.** Fundamental parameters of Qingjiang Cascade Station.

| Hydropower Station | Regulation Ability | Normal Water Level | Dead Water Level | Adjusted Capacity | Installed Capacity |
|---|---|---|---|---|---|
| **Unit** | **-** | **m** | **m** | **100 Million $m^3$** | **MW** |
| Shuibuya | Multi-year | 400.0 | 350 | 23.83 | 460 × 4 |
| Geheyan | Yearly | 200.0 | 161.2 | 19.75 | 300 × 4 |
| Gaobazhou | Daily | 80.0 | 78.0 | 0.512 | 84 × 3 |

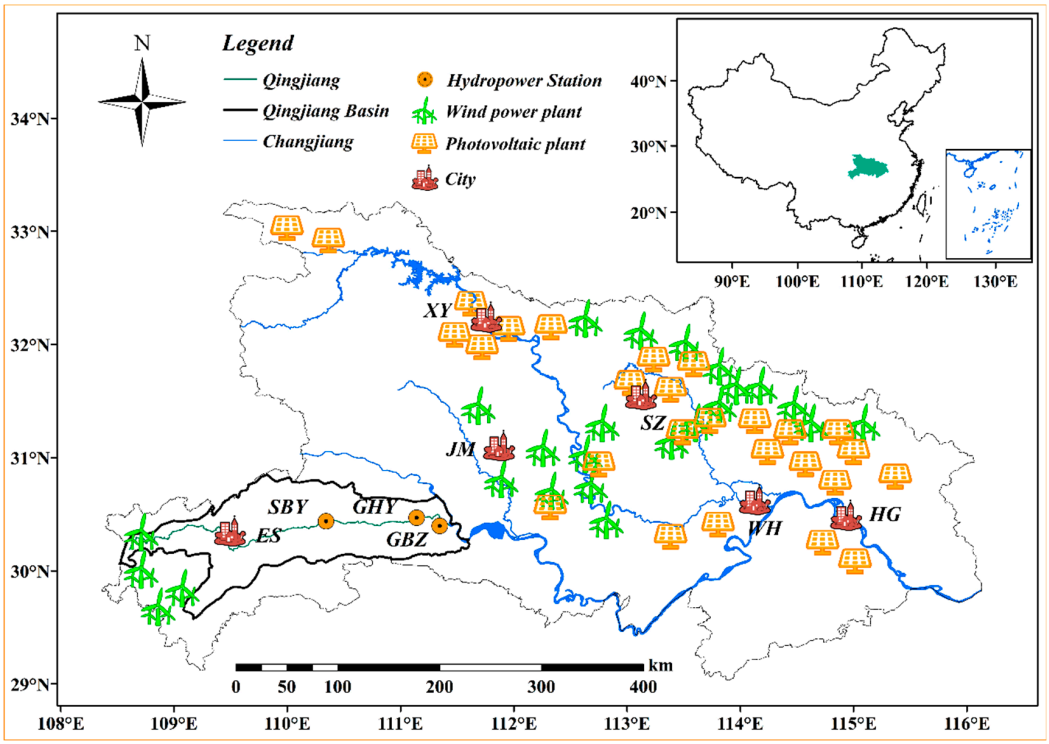



**Figure 2.** The schematic map of studied WPHSs in Hubei Province.

### *4.2. Data Description and Parameter Settings*

To evaluate the regulation performance of Qingjiang cascade hydropower stations on new energy output and grid load under different inflow conditions, this study selected 2 April 2019, the dry season, and 9 August 2019, the wet season, in the Qingjiang River Basin as typical day 1 (TD-1) and typical day 2 (TD-2). The hourly inflow and electricity consumption data on TD-1 and TD-2 were from the D5000 system of the central China branch of the State Grid Corporation of China.

A wind–solar virtual power plant is an energy management system that provides renewable energy power by integrating wind and solar resources. To simplify calculations, this study allocates the total installed wind power and photovoltaic capacity in the province to each virtual new energy power plant according to weight based on the installed density of wind power and solar power in each region of Hubei Province to estimate each virtual power plant. Table 2 summarizes the installed capacity of virtual wind, PV, and hydropower stations in Hubei Province. The production of wind energy and photovoltaic energy are related to the same time periods with two typical days in this study. The wind speed and photovoltaic radiation data utilized in this study are sourced from the European Center for Medium-Range Weather Forecasts (ECMWF). The data are provided on an hourly scale with accuracy at the county level. Figure 3 depicts the fluctuation in wind speed and photovoltaic radiation intensity for TD-1 and TD-2.

The population size was configured to 50, with a maximum of 5000 iterations, a crossover probability of 0.8, and a mutation probability of 0.03. Following the optimization concept and procedure of the MOCEA/D algorithm, the program was developed using Java on a Laptop-3crjhddf equipped with 16 GB RAM and an Intel Core i7-10750H CPU.

**Table 2.** Detailed distribution of power plants in the studied area.

| Plant Type | Number | Installed Capacity (MW) | Name | Symbol |
|---|---|---|---|---|
| Virtual wind power plant | 3 | 3311.9 | Enshi<br>Jingmen<br>Suizhou | W1<br>W2<br>W3 |
| Virtual PV plant | 3 | 3354.7 | Huanggang<br>Suizhou<br>Xiangyang | S1<br>S2<br>S3 |
| Hydropower plant | 3 | 3292 | Shuibuya<br>Geheyan<br>Gaobazhou | SBY<br>GHY<br>GBZ |

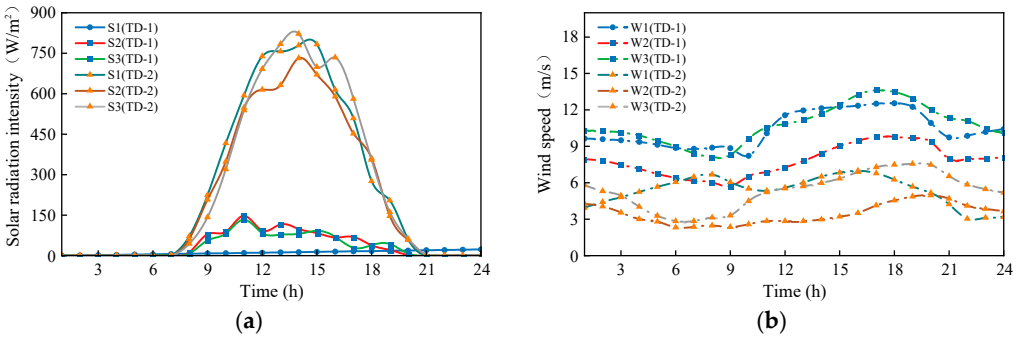



**Figure 3.** The process of wind speed and photovoltaic radiation intensity for virtual wind and photovoltaic plants in the study area during TD-1 and TD-2. (**a**) The process of wind speed; (**b**) The process of photovoltaic radiation intensity.

### *4.3. Result Analysis*

#### 4.3.1. Comparative Analysis of Load Characteristics on Two Typical Days

To visually display the difference in two typical days, the load curves of TD-1 and TD-2 are shown in Figure 4. It can be seen from the figure that for the power grid load process, the average load on TD-1 is about 20.81 million kW, while the average load on TD-2 is about 32.15 million kW. Therefore, the overall load level on TD-2 is significantly higher than that on TD-1. However, the load fluctuation index of the power grid on TD-1 reaches 0.103, which is higher than the load fluctuation level of 0.073 on TD-2, and there is less water inflow from the reservoir during the dry season. Therefore, this shows that the relative fluctuation degree of the power grid load on TD-1 is much higher than that on TD-2.

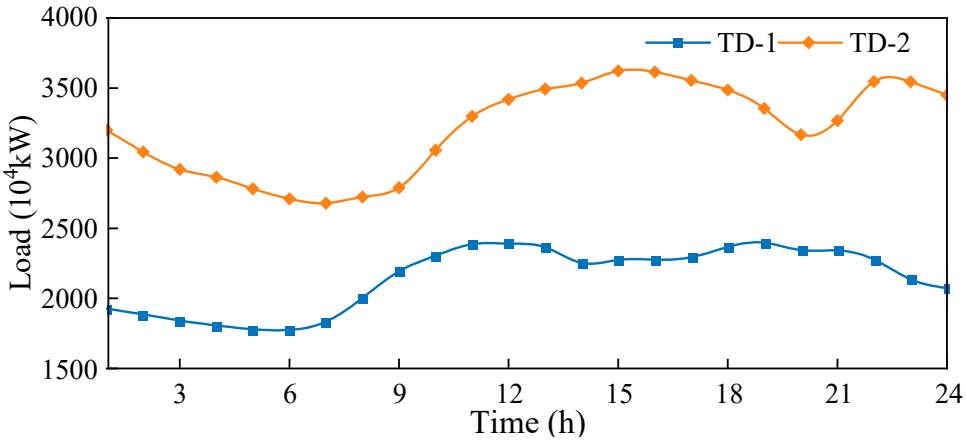



**Figure 4.** The load change process on TD-1 and TD-2.

4.3.2. Pareto Relationship between Two Objectives

The multi-objective optimal Pareto sets of the WPHSs in the dry season and flood season are plotted in Figure 5. Tables 3 and 4 respectively list the 50 detailed Pareto schemes under TD-1 and TD-2 scenarios. The smaller the mean square error of residual load, the better the peak-balancing effect. As evident from Figure 5, an increase in power generation benefits results in a corresponding increase in the root mean square error (RMSE) of the residual load. This indicates a decrease in the benefit of peak load balancing. Consequently, there exists a competitive relationship between these two objectives. The correlation in the noninferior sets between power generation and the mean square error of residual load reflects the interplay between the economic benefit of the power plant and the secure operation of the power grid.

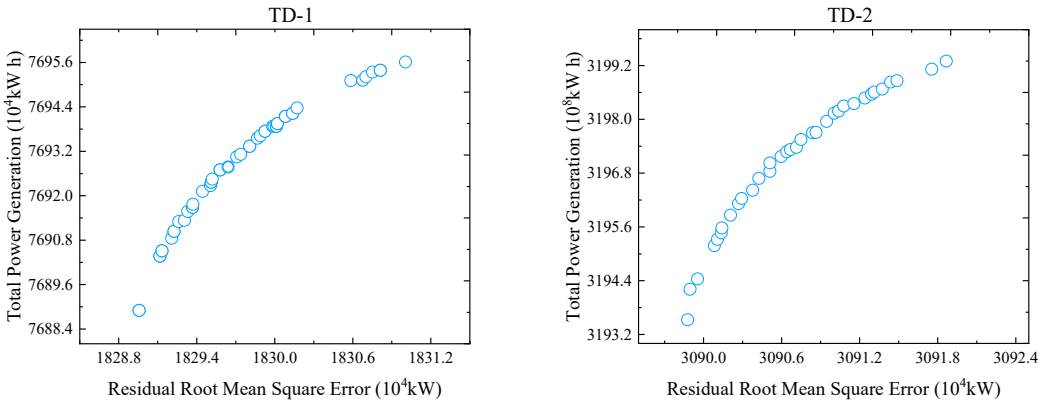



**Figure 5.** Pareto sets of the WPHSs on the TD-1 and TD-2. (**a**) TD-1; (**b**) TD-2.

**Table 3.** Detailed Pareto schemes under TD-1 scenario.

| Objective | Residual Load RMSE | Power Generation | Objective | Residual Load RMSE | Power Generation |
|---|---|---|---|---|---|
| Unit | $10^4$ kW | $10^4$ kW·h | Unit | $10^4$ kW | $10^4$ kW·h |
| 1 | 1828.957 | 7688.9021 | 26 | 1829.738 | 7693.1199 |
| 2 | 1828.957 | 7688.9021 | 27 | 1829.808 | 7693.3365 |
| 3 | 1829.116 | 7690.3705 | 28 | 1829.808 | 7693.3365 |
| 4 | 1829.116 | 7690.3705 | 29 | 1829.867 | 7693.5528 |
| 5 | 1829.132 | 7690.5111 | 30 | 1829.888 | 7693.6191 |
| 6 | 1829.132 | 7690.5111 | 31 | 1829.925 | 7693.7397 |
| 7 | 1829.208 | 7690.8513 | 32 | 1829.925 | 7693.7397 |
| 8 | 1829.225 | 7691.0355 | 33 | 1829.984 | 7693.8734 |
| 9 | 1829.225 | 7691.0355 | 34 | 1829.984 | 7693.8734 |
| 10 | 1829.261 | 7691.3003 | 35 | 1830.013 | 7693.8762 |
| 11 | 1829.305 | 7691.3347 | 36 | 1830.013 | 7693.8762 |
| 12 | 1829.331 | 7691.5761 | 37 | 1830.020 | 7693.9474 |
| 13 | 1829.368 | 7691.6869 | 38 | 1830.020 | 7693.9474 |
| 14 | 1829.368 | 7691.6869 | 39 | 1830.082 | 7694.1446 |
| 15 | 1829.371 | 7691.7676 | 40 | 1830.082 | 7694.1446 |
| 16 | 1829.444 | 7692.119 | 41 | 1830.138 | 7694.2258 |
| 17 | 1829.506 | 7692.2727 | 42 | 1830.138 | 7694.2258 |
| 18 | 1829.512 | 7692.3633 | 43 | 1830.172 | 7694.3711 |
| 19 | 1829.512 | 7692.3633 | 44 | 1830.585 | 7695.1106 |
| 20 | 1829.520 | 7692.4493 | 45 | 1830.677 | 7695.122 |
| 21 | 1829.580 | 7692.6981 | 46 | 1830.701 | 7695.2124 |
| 22 | 1829.580 | 7692.6981 | 47 | 1830.752 | 7695.3411 |
| 23 | 1829.641 | 7692.7752 | 48 | 1830.811 | 7695.3887 |
| 24 | 1829.641 | 7692.7752 | 49 | 1830.811 | 7695.3887 |
| 25 | 1829.707 | 7693.0496 | 50 | 1831.005 | 7695.6129 |

**Table 4.** Detailed Pareto schemes under TD-2 scenario.

| Objective | Residual Load RMSE | Power Generation | Objective | Residual Load RMSE | Power Generation |
|---|---|---|---|---|---|
| Unit | $10^4$ kW | $10^4$ kW·h | Unit | $10^4$ kW | $10^4$ kW·h |
| 1 | 3089.877 | 3193.5296 | 26 | 3090.714 | 3197.377 |
| 2 | 3089.896 | 3194.2096 | 27 | 3090.749 | 3197.5519 |
| 3 | 3089.896 | 3194.2096 | 28 | 3090.749 | 3197.5519 |
| 4 | 3089.954 | 3194.4412 | 29 | 3090.837 | 3197.6987 |
| 5 | 3090.083 | 3195.1838 | 30 | 3090.837 | 3197.6987 |
| 6 | 3090.083 | 3195.1838 | 31 | 3090.865 | 3197.7103 |
| 7 | 3090.107 | 3195.3224 | 32 | 3090.946 | 3197.9541 |
| 8 | 3090.107 | 3195.3224 | 33 | 3091.003 | 3198.1368 |
| 9 | 3090.136 | 3195.4690 | 34 | 3091.039 | 3198.1865 |
| 10 | 3090.141 | 3195.5780 | 35 | 3091.039 | 3198.1865 |
| 11 | 3090.208 | 3195.8630 | 36 | 3091.078 | 3198.298 |
| 12 | 3090.208 | 3195.8630 | 37 | 3091.078 | 3198.298 |
| 13 | 3090.269 | 3196.1209 | 38 | 3091.156 | 3198.3512 |
| 14 | 3090.269 | 3196.1209 | 39 | 3091.156 | 3198.3512 |
| 15 | 3090.293 | 3196.2357 | 40 | 3091.242 | 3198.477 |
| 16 | 3090.378 | 3196.4207 | 41 | 3091.242 | 3198.477 |
| 17 | 3090.378 | 3196.4207 | 42 | 3091.291 | 3198.5608 |
| 18 | 3090.426 | 3196.6840 | 43 | 3091.312 | 3198.6083 |
| 19 | 3090.509 | 3196.8423 | 44 | 3091.312 | 3198.6083 |
| 20 | 3090.510 | 3197.0271 | 45 | 3091.374 | 3198.6753 |
| 21 | 3090.596 | 3197.1728 | 46 | 3091.438 | 3198.8311 |
| 22 | 3090.596 | 3197.1728 | 47 | 3091.487 | 3198.8631 |
| 23 | 3090.640 | 3197.2772 | 48 | 3091.753 | 3199.1176 |
| 24 | 3090.669 | 3197.3250 | 49 | 3091.753 | 3199.1176 |
| 25 | 3090.714 | 3197.3770 | 50 | 3091.867 | 3199.2977 |

According to the Pareto curve of two typical days, three typical schemes are selected equidistantly from left to right. The curve on the left side of scheme II exhibits a trend towards minimizing the residual load mean square error, while the inclination on the right side is to increase power generation. These trends are observable in both the dry season and the flood season. Consequently, the change process of these three typical schemes can be intuitively reflected in the alteration between the power generation benefit and the peaking benefit target in the Pareto front. The schemes on TD-1 and TD-2 show similar changing patterns. To avoid redundancy, TD-1 is used as an example for detailed analysis. Compared with scheme I, the power generation and residual load mean square error of scheme II increased by 41,475 kWh and 7499 kW, respectively. Compared with scheme III, the power generation and residual load mean square error of scheme II are reduced by 25,633 kWh and 12,980 kW, respectively. This can be attributed to the different optimization emphasis of each scheme on the two objectives.

#### 4.3.3. Analysis of the Effect of Cascade Hydropower Scheduling on the Operation of WPHSs

To visually display the dispatching process of a typical scheme, the wind power, photovoltaic, and hydropower output processes, grid load, and grid residual load of the typical schemes are depicted in Figures 6 and 7. Figures 6 and 7 illustrate that upon connecting the hydro–wind–solar combined system to the power grid, the fluctuation amplitude of the grid residual load under the three typical scenarios on TD-1 and TD-2 is noticeably reduced compared to the original load process. Among the schemes, scheme I demonstrate the most stable residual load process, particularly during the hours of 10–18 on TD-1 and TD-2. This stability is attributed to scheme I prioritizing peak-shaving benefits in its multi-objective optimization, leading to the highest peak-shaving efficiency and the most stable residual load. However, this comes at the expense of sacrificing some generation efficiency. During the hours of 3–6 and 12–17 on TD-1, as well as 9–18 on

TD-2, these periods align with low grid demand and high photovoltaic output. In these instances, the residual load process aims to minimize amplitude while preserving stability. The cascade hydropower station achieves this by decreasing spillage to lower output and conserve water during these periods. Figures 8 and 9 show the process of water level and discharge of the cascaded hydropower station after optimizing TD-1 and TD-2. The cascaded hydropower station reduces the output and stores water by reducing the discharge flow. The water level-flow diagram reveals that SBY, as the primary power station in the Qingjiang cascade, is responsible for a larger share of power generation plans. SBY reduces the output by reducing the discharge flow and stores water to a higher level to provide sufficient water for subsequent periods and improve power generation efficiency; GHY also discharges with a small discharge flow. Due to its limited regulation and storage capacity, GBZ exhibits a small output fluctuation and generates power in a relatively straight line. In summary, the outflow flow process of each hydropower station is consistent with the output process. However, during the hours of 6–10 and 19–21 on TD-1, as well as 21–23 on TD-2, these periods align with peak grid demand, with low photovoltaic and wind output. Cascade hydropower stations increase the discharge flow to boost hydropower output during peak load operation. Hence, the output process of Qingjiang cascade hydropower stations under varying incoming water conditions adeptly tracks changes in grid load and new energy output. This effectively stabilizes wind power, photovoltaic output, and grid load fluctuations, ultimately achieving the goal of promoting wind power and photovoltaic consumption.

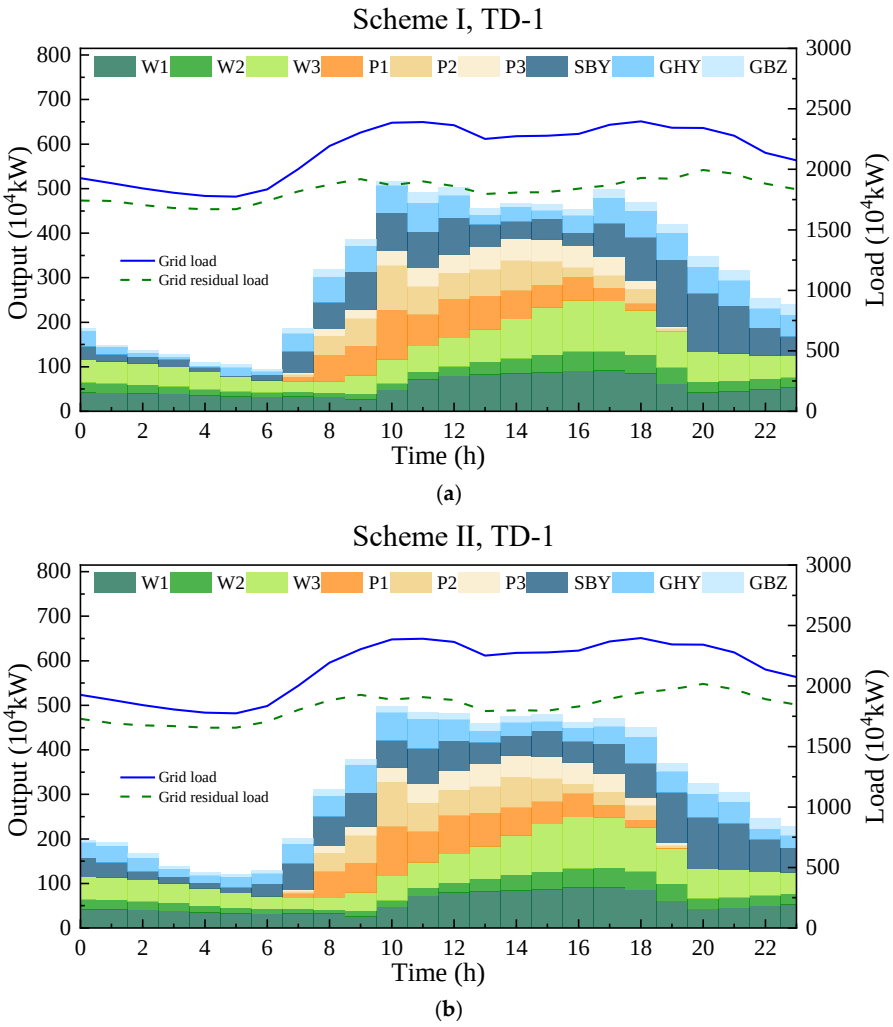
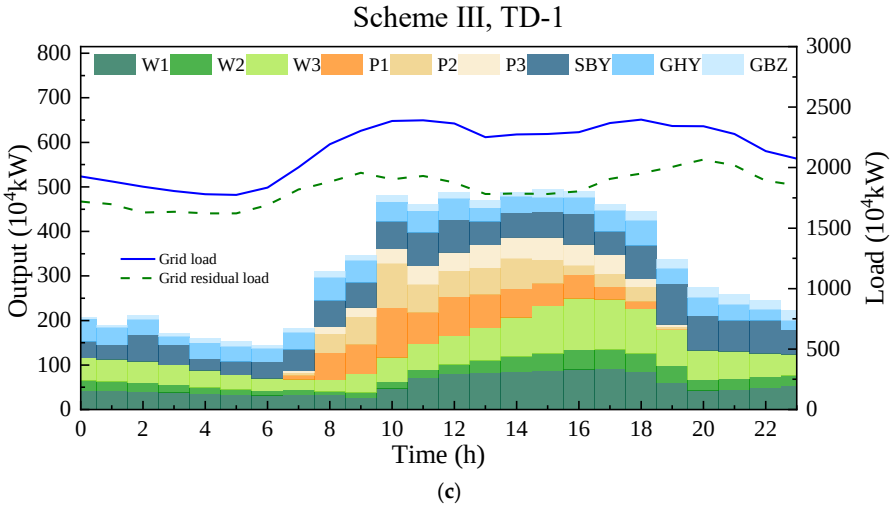



**Figure 6.** *Cont.*




(**c**)

**Figure 6.** Output and load process after connecting to the WPHSs on TD-1. (**a**) Scheme I on TD-1; (**b**) Scheme II on TD-1; (**c**) Scheme III on TD-1.

#### 4.3.4. Evaluation of the Effect of Cascade Hydropower on Power Grid Load Regulation

To quantitatively assess the peak-shaving effect, this paper introduces three indicators: load peak–valley difference, mean square error, and load rate. These indicators evaluate the regulating effect of the Qingjiang cascade hydropower stations on new energy output and the peak-shaving performance of the grid load. Peak–valley difference characterizes the amplitude of load variations; mean square deviation quantifies the volatility of load fluctuations, reflecting the smoothness of details in the load process; load rate characterizes the load variation, reflecting the stability of the load process at a global time scale. Smaller peak–valley differences and mean square error indicate smoother load processes, while the load factor values are the opposite.

Taking scheme I on two typical days as an example, Table 5 presents the original load, equivalent load, and residual load index values after the cascade hydropower peaking for illustrative purposes. Analysis of the table indicates that after the connection of wind power and photovoltaics, the equivalent load peak-to-valley difference between TD-1 and TD-2 is slightly smaller than the original load of the power grid. However, the mean square error and load rate are slightly higher than the original load. In contrast to the load process after the integration of hydropower into the power grid, the peak–valley difference and mean square error experienced a notable reduction. Compared with the original load on TD-1, the peak–valley difference and mean square error of residual load dropped by 47.69% and 51.58%, respectively, the load factor increased by 2.21%, and the peak-cutting depth was 191.94 million kWh. Compared with the original load on TD-2, the peak–valley difference and mean square error of residual load dropped by 20.28% and 25.25%, respectively, the load factor increased by 1.79%, and the peak-cutting depth was 117.31 million kWh. The results suggest that for different typical days, the grid residual load process after hydropower peak shaving is more stable than the grid residual load process after only new energy is connected. This highlights the significant peak-shaving performance of cascade hydropower stations.

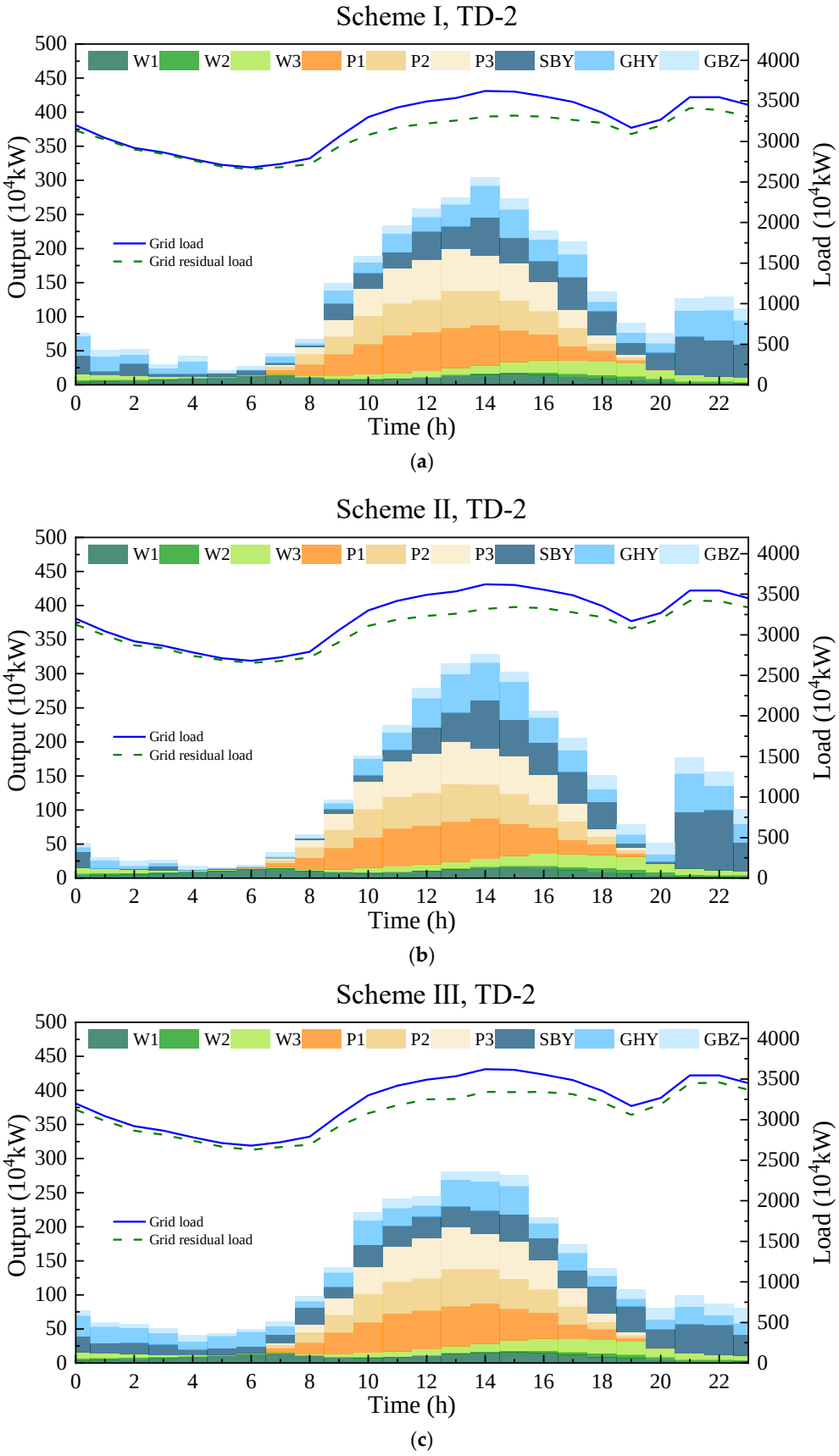



**Figure 7.** Output and load process after connecting to the WPHSs on TD-2. (**a**) Scheme I on TD-2; (**b**) Scheme II on TD-2; (**c**) Scheme III on TD-2.

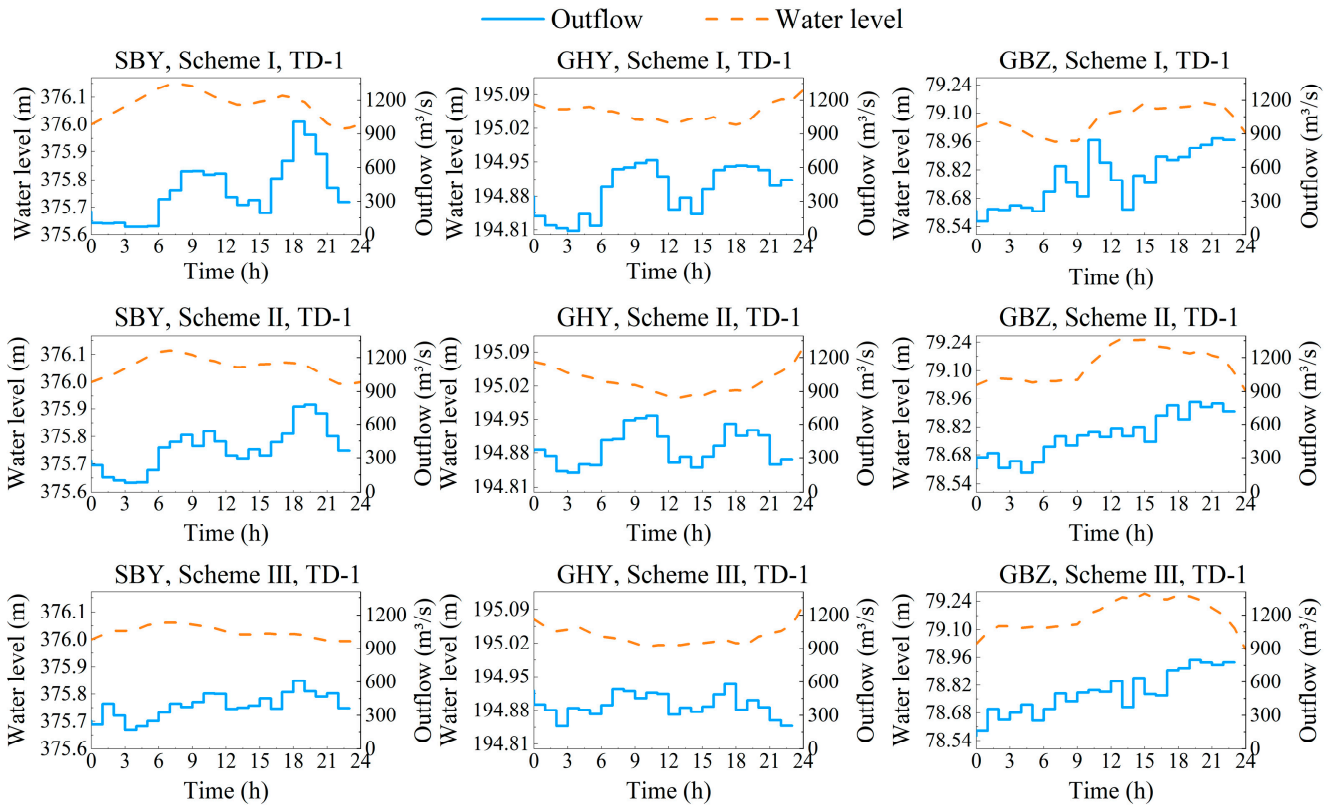



**Figure 8.** Water level discharge process of Qingjiang cascaded reservoirs on TD-1.

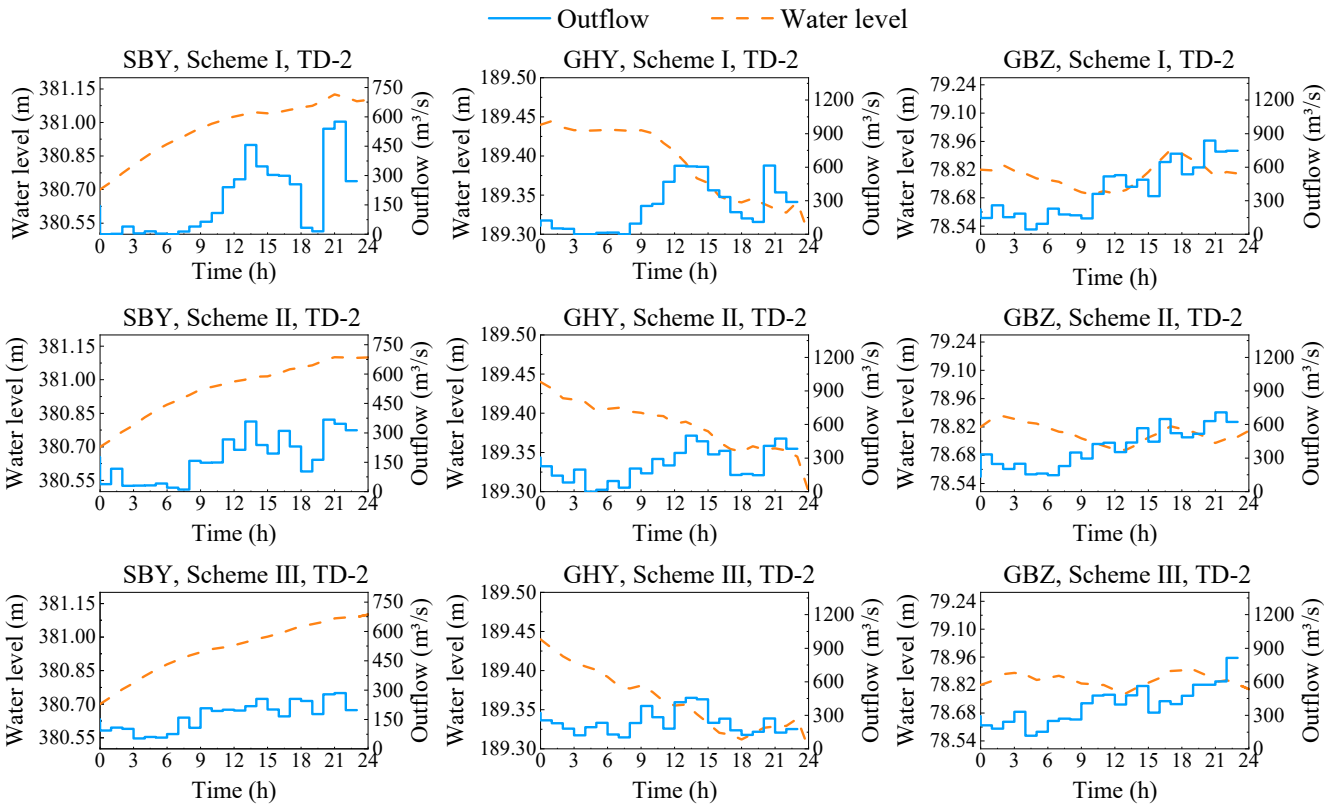



**Figure 9.** Water level discharge process of Qingjiang cascaded reservoirs on TD-2.

**Table 5.** Comparison of power grid load process indicators.

| Indicator | Peak-to-Valley Difference (Million kW) | | Mean Square Error (Million kW) | | Load Rate (%) | |
|---|---|---|---|---|---|---|
| **Load Type/Day Type** | **TD-1** | **TD-2** | **TD-1** | **TD-2** | **TD-1** | **TD-2** |
| Original load | 622.02 | 942.96 | 226.95 | 327.13 | 89.96 | 88.72 |
| Equivalent load | 607.88 | 869.01 | 154.93 | 288.47 | 87.66 | 88.86 |
| Residual load | 514.99 | 751.70 | 93.45 | 244.52 | 91.54 | 90.29 |
| Difference (%) | −47.69 | −20.28 | −58.82 | −25.25 | 1.75 | 1.76 |
| Peak-cutting depth | 191.94 | 117.31 | - | - | - | - |

(1) Equivalent load denotes the temporal curve depicting the original total load of the entire network subtracted by the output of wind and photovoltaic power. (2) Peak-cutting depth denotes the difference between the peak-to-valley difference of the equivalent load and the peak-to-valley difference of the residual load. (3) Difference denotes the degree of optimization of the residual load relative to the original load.

## 5. Conclusions and Future Work

Compensating wind and solar power with hydropower proves to be an effective approach to addressing the challenges of clean energy integration. In response to the large-scale integration of new energy sources into provincial power grids and the coordination issues between WPHSs and the secure operation of the power grid, this study proposes a multi-objective coordination optimization scheduling model for the power plant network. The optimization objectives prioritize maximizing the generation output of complementary systems and minimizing the mean square deviation of the receiving-end power grid load. The model was validated using WPHSs in Hubei Province, China, and the Pareto optimal scheme set was acquired. The results of the model calculations for typical days during the dry and wet periods of the hydropower station reveal a conspicuous competition relationship between the total generation of the basin hydro–photovoltaic system and the smoothness of the power grid load. Additionally, the results also indicate that the output process of the Qingjiang cascade hydropower stations, under varying water inflow conditions, effectively tracks changes in power grid load and new energy output. This characteristic effectively dampens the fluctuations in wind and solar power output and smooths the curves of the power grid load. In summary, this study proposes a short-term multi-energy complementary optimization model for hydro–photovoltaic systems, considering source–grid coordination. The research delves into the relationships between objectives and the coordination mechanism of cascade hydropower in complementary systems.

This paper mainly studies the coordination problem between the hydro–wind–solar hybrid system and the average load during hourly periods under centralized dispatch conditions. Regarding the coordination problem under power market conditions and the development of energy storage in the future, the multi-objective coordination of hydro–wind–solar storage still needs further research.

**Author Contributions:** Conceptualization, Q.S. and L.M.; methodology, Q.S.; software, Q.S.; validation, Z.L., X.S. and G.L.; formal analysis, Q.S.; data curation, Z.L.; writing—original draft preparation, Q.S.; writing—review and editing, supervision, Y.Z.; funding acquisition, L.M. All authors have read and agreed to the published version of the manuscript.

**Funding:** This research is supported by the National Natural Science Foundation of China (No. 52379011) and the APC was funded by the National Natural Science Foundation of China (No. 52379011).

**Institutional Review Board Statement:** Not applicable.

**Informed Consent Statement:** Not applicable.

**Data Availability Statement:** Data will be made available on request.

**Conflicts of Interest:** The authors declare no conflict of interest.

## References


1. Lei, K.; Chang, J.; Wang, X.; Guo, A.; Wang, Y.; Ren, C. Peak shaving and short-term economic operation of hydro-wind-PV hybrid system considering the uncertainty of wind and PV power. *Renew. Energy* **2023**, *215*, 118903. [CrossRef]
2. Wang, H.; Lu, X.; Deng, Y.; Sun, Y.; Nielsen, C.P.; Liu, Y.; Bu, M.; Bi, J.; McElroy, M.B. China's $CO_2$ peak before 2030 implied from characteristics and growth of cities. *Nat. Sustain.* **2019**, *2*, 748–754. [CrossRef]
3. National Development and Reform Commission of the People's Republic of China. *China to Pilot Carbon-Peaking in 100 Cities, Zones*; National Development and Reform Commission of the People's Republic of China: Beijing, China, 2023.
4. Zhang, Z.; Qin, H.; Li, J.; Liu, Y.; Yao, L.; Wang, Y.; Wang, C.; Pei, S.; Zhou, J. Short-term optimal operation of wind-solar-hydro hybrid system considering uncertainties. *Energy Conv. Manag.* **2020**, *205*, 112405. [CrossRef]
5. Karadöl, İ.; Yıldız, C.; Şekkeli, M. Determining optimal spatial and temporal complementarity between wind and hydropower. *Energy* **2021**, *230*, 120790. [CrossRef]
6. Wei, H.; Hongxuan, Z.; Yu, D.; Yiting, W.; Ling, D.; Ming, X. Short-term optimal operation of hydro-wind-solar hybrid system with improved generative adversarial networks. *Appl. Energy* **2019**, *250*, 389–403. [CrossRef]
7. Biswas, P.P.; Suganthan, P.N.; Qu, B.Y.; Amaratunga, G.A. Multiobjective economic-environmental power dispatch with stochastic wind-solar-small hydro power. *Energy* **2018**, *150*, 1039–1057. [CrossRef]
8. Liu, W.; Zhu, F.; Chen, J.; Wang, H.; Xu, B.; Song, P.; Zhong, P.; Lei, X.; Wang, C.; Yan, M.; et al. Multi-objective optimization scheduling of wind–photovoltaic–hydropower systems considering riverine ecosystem. *Energy Conv. Manag.* **2019**, *196*, 32–43. [CrossRef]
9. Wang, X.; Chang, J.; Meng, X.; Wang, Y. Hydro-thermal-wind-photovoltaic coordinated operation considering the comprehensive utilization of reservoirs. *Energy Conv. Manag.* **2019**, *198*, 111824. [CrossRef]
10. Wang, K.Y.; Luo, X.J.; Wu, L.; Liu, X.C. Optimal coordination of wind-hydro-thermal based on water complementing wind. *Renew. Energy* **2013**, *60*, 169–178. [CrossRef]
11. Glasnovic, Z.; Margeta, K.; Premec, K. Could Key Engine, as a new open-source for RES technology development, start the third industrial revolution? *Renew. Sustain. Energy Rev.* **2016**, *57*, 1194–1209. [CrossRef]
12. Destro, N.; Korpås, M.; Sauterleute, J.F. Smoothing of offshore wind power variations with Norwegian pumped hydro: Case study. *Energy Procedia* **2016**, *87*, 61–68. [CrossRef]
13. Zhu, F.; Zhong, P.A.; Xu, B.; Liu, W.; Wang, W.; Sun, Y.; Chen, J.; Li, J. Short-term stochastic optimization of a hydro-wind-photovoltaic hybrid system under multiple uncertainties. *Energy Conv. Manag.* **2020**, *214*, 112902. [CrossRef]
14. Liu, B.; Lund, J.R.; Liao, S.; Jin, X.; Liu, L.; Cheng, C. Optimal power peak shaving using hydropower to complement wind and solar power uncertainty. *Energy Conv. Manag.* **2020**, *209*, 112628. [CrossRef]
15. Sulaiman, M.H.; Mustaffa, Z. Solving optimal power flow problem with stochastic wind–solar–small hydro power using barnacles mating optimizer. *Control Eng. Pract.* **2021**, *106*, 104672. [CrossRef]
16. Javed, M.S.; Ma, T.; Jurasz, J.; Amin, M.Y. Solar and wind power generation systems with pumped hydro storage: Review and future perspectives. *Renew. Energy* **2020**, *148*, 176–192. [CrossRef]
17. Jin, X.; Liu, B.; Liao, S.; Cheng, C.; Li, G.; Liu, L. Impacts of different wind and solar power penetrations on cascade hydroplants operation. *Renew. Energy* **2022**, *182*, 227–244. [CrossRef]
18. Wang, X.; Mei, Y.; Kong, Y.; Lin, Y.; Wang, H. Improved multi-objective model and analysis of the coordinated operation of a hydro-wind-photovoltaic system. *Energy* **2017**, *134*, 813–839. [CrossRef]
19. Zhang, J.; Cheng, C.; Shen, J.; Li, G.; Li, X.; Zhao, Z. Short-term Joint Optimal Operation Method for High Proportion Renewable Energy Grid Considering Wind-solar Uncertainty. *Proc. CSEE* **2020**, *40*, 5921–5931. [CrossRef]
20. Zhang, Y.; Lian, J.; Ma, C.; Yang, Y.; Pang, X.; Wang, L. Optimal sizing of the grid-connected hybrid system integrating hydropower, photovoltaic, and wind considering cascade reservoir connection and photovoltaic-wind complementarity. *J. Clean. Prod.* **2020**, *274*, 123100. [CrossRef]
21. Li, T.; Huang, Z.; She, S. Analysis of hybrid wind-photovoltaic-hydro generation system based on short-term scheduling. *J. Phys. Conf. Ser.* **2020**, *1549*, 52006. [CrossRef]
22. Wang, X.; Virguez, E.; Xiao, W.; Mei, Y.; Patiño-Echeverri, D.; Wang, H. Clustering and dispatching hydro, wind, and photovoltaic power resources with multiobjective optimization of power generation fluctuations: A case study in southwestern China. *Energy* **2019**, *189*, 116250. [CrossRef]
23. Tan, Q.; Wen, X.; Sun, Y.; Lei, X.; Wang, Z.; Qin, G. Evaluation of the risk and benefit of the complementary operation of the large wind-photovoltaic-hydropower system considering forecast uncertainty. *Appl. Energy* **2021**, *285*, 116442. [CrossRef]
24. Zhang, X.; Huang, W.; Chen, S.; Xie, D.; Liu, D.; Ma, G. Grid–source coordinated dispatching based on heterogeneous energy hybrid power generation. *Energy* **2020**, *205*, 117908. [CrossRef]
25. Zhang, X.; Ma, G.; Huang, W.; Chen, S.; Zhang, S. Short-term optimal operation of a wind-PV-hydro complementary installation: Yalong River, Sichuan Province, China. *Energies* **2018**, *11*, 868. [CrossRef]
26. Vargas, S.A.; Esteves, G.R.T.; Maçaira, P.M.; Bastos, B.Q.; Oliveira, F.L.C.; Souza, R.C. Wind power generation: A review and a research agenda. *J. Clean. Prod.* **2019**, *218*, 850–870. [CrossRef]
27. Qiu, T.; Wang, L.; Lu, Y.; Zhang, M.; Qin, W.; Wang, S.; Wang, L. Potential assessment of photovoltaic power generation in China. *Renew. Sustain. Energy Rev.* **2022**, *154*, 111900. [CrossRef]

28. Ming, B.; Liu, P.; Guo, S.; Cheng, L.; Zhang, J. Hydropower reservoir reoperation to adapt to large-scale photovoltaic power generation. *Energy* **2019**, *179*, 268–279. [CrossRef]
29. Zhang, Q.; Li, H. MOEA/D: A multiobjective evolutionary algorithm based on decomposition. *IEEE Trans. Evol. Comput.* **2007**, *11*, 712–731. [CrossRef]
30. Reynolds, R.G. An introduction to cultural algorithms. In Proceedings of the 3rd Annual Conference on Evolutionary Programming, San Diego, CA, USA, 24–26 February 1994; World Scientific Publishing: Singapore, 1994; pp. 131–139.

**Disclaimer/Publisher's Note:** The statements, opinions and data contained in all publications are solely those of the individual author(s) and contributor(s) and not of MDPI and/or the editor(s). MDPI and/or the editor(s) disclaim responsibility for any injury to people or property resulting from any ideas, methods, instructions or products referred to in the content.